International Journal of Power Electronics and Drive Systems (IJPEDS)
Vol. 15, No. 1, March 2024, pp. 281~291
ISSN: 2088-8694, DOI: 10.11591/ijpeds.v15.i1.pp281-291

The use of a front-end ZVZCS DC-DC converter for an IoT VFD inverter system in the paddle wheel machine drive applications

Nitthita Chirdchoo[1], Watanyu Meesrisuk[1], Weerasak Chuenta[2]
[1]Department of Electrical Engineering, Faculty of Science and Technology, Nakhon Pathom Rajabhat University, Nakhon Pathom, Thailand
[2]Department of Intelligent Control Innovation, Faculty of Science and Technology, Nakhon Pathom Rajabhat University, Nakhon Pathom, Thailand

Article Info

Article history:

Received Apr 18, 2023
Revised Jun 28, 2023
Accepted Jul 20, 2023

Keywords:

IoT system
Shrimp farming
The front-end converter
VFD inverter
ZVZCS

ABSTRACT

This research paper proposes the integration of power electronics and internet of things (IoT) technologies to apply in shrimp farms. By focusing on the design of a front-end converter, a three-level half-bridge (3L-HB) DC-DC converter with the zero voltage and zero current switching (ZVZCS) technique is chosen to be the front-end power converter to supply the DC bus voltage for the variable frequency drive (VFD) inverter for the paddle wheel machine in the shrimp pond. To confirm the effectiveness and possibility of the proposed concept, the circuit was theoretically designed and tested at 540 Vdc of the input voltage, 700 Vdc of the DC bus voltage and 3 kW of rated power. It is found that, the front-end converter can step up the DC bus to be 700 Vdc which is enough for operating the VFD inverter. All switches can achieve the soft switching condition ZVZCS resulting in decreasing the switching loss and increasing the reliability of the circuit. The maximum experimental efficiency of the front-end converter is 94.9% at 75% of a full load. In addition, the introductory concept of using the IoT system also presents to improve the shrimp farming method.

Corresponding Author:

Watanyu Meesrisuk
Department of Electrical Engineering, Faculty of Science and Technology
Nakhon Pathom Rajabhat University
Nakhon Pathom, Thailand
Email: watanyu@webmail.npru.ac.th

1. INTRODUCTION

- Motivation and incitement

Nowadays, shrimp farming could be considered as one of the main agricultural industry in Thailand. From the report of department of trade negotiations Thailand in 2022, Thailand is the 6th fresh shrimp exporter of the world with 1,577.6 million US dollars of total export value. From the fact that, Thailand used to be the 1st fresh shrimp exporter of the world during the period from 2007 to 2012. However, the lack of the competitive ability of Thailand in the last few years are the results of the inefficient management and the higher production cost comparing to the other country. Due to most shrimp farms in Thailand are small and medium farms, they still use traditional methods without any new technology because of the shortage of capital and they do not understand the problems from the past round.

- Literature review

From the climate change issue, many shrimp farms have changed the type of energy sources from the diesel fuel to electric energy for controlling paddle wheel machines which are used in shrimp ponds to maintain the quality of water dissolved oxygen (DO) and temperature in the pond to be appropriate for shrimp growth. Most of the farms use the classical motor control method such as on-off control and direct online starting (DOL) technique to control the induction motor of the paddle wheel machine because these techniques are simple and economical whereas they still have found some problems that waste their capital. For instance, the classical motor control method is not able to directly adjust the speed of the motor. They have to use the gearbox for changing the paddle wheel speed. This results in increasing the mechanical loss and decreasing the total efficiency of the system. Furthermore, the main drawback of DOL technique is the high starting current (about 5-7 times of the rated current) [1], which is the cause of the voltage dip in power line [2]–[6] resulting in the failure of other electric devices. To overcome the mentioned problems, a variable frequency drive (VFD) [7]–[10] inverter has been chosen to apply with the paddle wheel machine because it can easily adjust the speed of the induction motor. However, one of the major problems of using the VFD inverter is the under-voltage condition at the DC bus resulting in the overcurrent situation in the coils of the induction motor. The conventional VFD inverter uses boost DC-DC converter [11]–[17] to step up the DC bus to be appropriate with the requirement of the VFD inverter (about 600–700 V). Although boost converter can provide the desirable DC bus voltage, the main switch has to endure high power, high voltage, and high current stresses that can cause the failure of the VFD inverter.

In order to deal with this important problem, many power DC-DC converters with soft switching techniques have been proposed in [18]–[20] which presents the zero-voltage switching technique (ZVS) to reduce the switching losses of switching devices at the turning on time. However, the ZVS technique cannot eliminate all switching losses. It still has switching losses at turning off time. To overcome this critical problem, the zero-voltage and zero-current switching technique (ZVZCS) has been suggested in the past researches [21]–[27] that can decrease the voltage stress and current stress on main switches resulting in directly decreasing switching losses of DC-DC converters. From literature reviews, this research will choose the three-level ZVZCS topology [28]–[32] to apply with the VFD inverter for the paddle wheel machine as the front-end converter because of some advantages such as high stability and high efficiency due to lower voltage and current stress on main switching devices, and high safety for the user due to the isolation of the high frequency transformer.

- Contribution and paper organization

Furthermore, another objective of this research is to motivate shrimp farmers in Thailand to emphasize how important is it for the new technology to improve their shrimp farming. Internet of things (IoT) [33]–[36] will be also applied in this research because it can provide data from electronic devices such as sensors, microcontrollers to users via the internet. This advantage can improve the management of shrimp farming and help farmers to decide in controlling of the paddle wheel machine by using the data from the IoT system. Based on the above information, this research will propose the concept to integrate the application of power electronics, IoT systems, and agriculture for improving the method of shrimp farming [37], [38]. However, this paper will only focus on designing the front-end ZVZCS DC-DC converter for applying to an IoT VFD Inverter system in the shrimp pond.

2. THEORETICAL BASIS AND METHOD

2.1. The structure of this research

Figure 1 illustrates the structure of the IoT VFD inverter system which composes of many parts as follows. Firstly, a VFD inverter generates the suitable three-phase voltage waveforms and supplies them to the induction motor of the paddle wheel machine in shrimp ponds. At the front side of the VFD inverter, the front-end ZVZCS DC-DC converter [39] is used to regulate the DC bus voltage to be appropriate with the input voltage specification of the VFD inverter. The related data and some parameters are detected and measured by sensors that can be divided into 2 parts: i) the quality of water and ii) electrical data. The quality of water consists of pH, temperature, and dissolved oxygen (DO). The electrical data are the DC bus voltage, the measured voltage, current and frequency values of the induction motor, respectively. These data will be transmitted to the IoT system via the microcontroller and then the data will be sent to the host server via the internet. The host server will collect all data and monitor it to users or farmers via the web application system. Farmers can easily access the data of the shrimp pond by electronic devices such as the laptop or the smart phone. From the data, farmers can decide to control the paddle wheel machine to maintain the quality of water for shrimp growth.

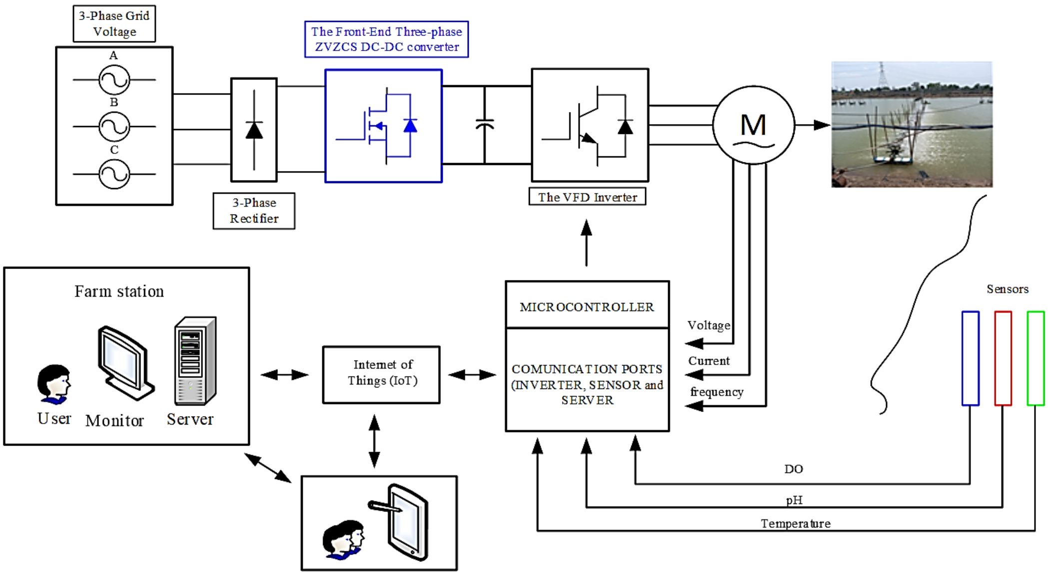

Figure 1. The structure of the proposed IoT VFD inverter system

2.2. The front-end ZVZCS DC-DC converter

Figure 2 illustrates the power conversion circuit of the IoT VFD inverter system that consists of 2 parts (the front-end and the VFD inverter). The front-end converter is the three-level half-bridge ZVZCS DC-DC converter and the VFD inverter is the conventional insulated-gate bipolar transistor (IGBT) inverter which are not mentioned in detail in this paper. The front-end converter receives the DC input voltage ($V_{dc,in}$) from the 3-phase rectifier circuit which is connected to the grid voltage source. The DC input voltage ($V_{dc,in}$) is divided to be 3-level voltage (0, $V_{dc}/2$ and V_{dc}) by both dividing capacitors (C_{dc1} and C_{dc2}) before directly supplied to the 3L-HB inverter. The 3L-HB inverter consists of 4 MOSFETs (S_1 – S_4) that generate the high frequency voltage. At the output side of the inverter, the step-up high frequency transformer (Tr) with the leakage inductor (L_{lk}) is used for stepping up the high frequency voltage, and the output bridge rectifier (D_{rec1} – D_{rec4}) is used for converting the secondary voltage waveform to be the DC voltage waveform. At the output of the front-end converter, there is the auxiliary circuit (D_{aux1}, D_{aux2} and C_{aux}) for completely achieving the ZCS condition for main switching devices. The output capacitor (C_o) is used for filtering the DC output voltage before supplied to the VFD inverter. Finally, the conventional IGBT inverter (Q_1 – Q_6) is chosen to be the VFD inverter for driving the induction motor of the paddle wheel machine.

At the DC bus, the dynamic braking circuit (IGBT, Q_b and braking resistor, R_b) is used for protecting the capacitor C_o from the failure in case of the DC bus voltage exceeds the limitation of rated voltage while the induction motor decreases the speed or brakes. Figure 3 shows some waveforms of the front-end converter which consists of PWM signals (G_1 – G_4) for all MOSFETs, the primary voltage (V_{ab}) and the primary current (i_a) waveforms of the high frequency transformer, the voltage, and the current waveforms of MOSFETs (S_1 and S_2). It is found that, the phase-shift pulse width modulation scheme (PSPWM) is used for controlling the output voltage of the front-end converter. In addition, the ZVS and ZCS patterns can be observed on the waveforms of MOSFETs (S_1 and S_2). Due to this paper aims to apply the ZVZCS DC-DC converter to the VFD inverter, the operation mode will not be mentioned in details. However, the operation mode of the circuit has been described in [26], [27].

2.3. Design consideration of the front-end ZVZCS DC-DC converter

To design all parameters of the proposed front-end converter for the VFD inverter, the specifications of the circuit can be defined as follows: i) The rated power $P_{front\text{-}end}$ = 3 kW, the DC input voltage $V_{dc,in}$ = 540 V; ii) The DC bus voltage at the output side of the front-end converter (DC Bus) $V_{dc,bus}$ = 700 V; and iii) The switching frequency f_{sw} = 65 kHz (the period T_s = 15.4 μs). Due to the use of PSPWM scheme in the front-end converter at any phase-shift angle time (θ), the ideal rectified voltage waveform at the front of the DC bus can be considered as shown in Figure 4(a) and calculated by (1).

$$V_{dc,bus} = \frac{v_{sec,max}\times(0.5T_S-\theta)}{0.5T_S} \tag{1}$$

According to (1), the maximum secondary voltage of T_r can be rearranged as (2).

$$V_{sec,max} = \frac{V_{dc,bus} \times 0.5T_s}{0.5T_s - \theta} \quad (2)$$

The maximum primary voltage of T_r can be given by (3).

$$V_{pri,max} = \frac{V_{dc,in}}{2} \quad (3)$$

According to (2) and (3), the turn ratio of T_r can be given by (4).

$$n = \frac{V_{dc,in}(1-\frac{2\theta}{T_s})}{2V_{dc,bus}} \quad (4)$$

Let θ = 5.12 μs (about 60 degree of phase-shifted angle) which can provide the maximum DC bus voltage at 700 V, thus the turn ratio of the high frequency transformer (T_r) can be calculated by (5).

$$n = \frac{540(1-\frac{2(5.12)}{15.4})}{2(700)} = 0.13 \quad (5)$$

According to (5), the high-frequency transformer (T_r) was designed using the area product method (AP method). From the design, a number of turns of primary and secondary coils equal to 5 and 38 turns, respectively and then the T_r was measured by the impedance analyzer to find its parameters, the leakage inductor (L_{lk}) of T_r equals to 22 μH. On the part of selecting all semiconductor devices in the circuit, the rating of them was calculated by considering the safety factors. The IRFP460 (20 A and 500 V) was chosen as all MOSFETs ($S_1 - S_4$) and the RHRP30120 (30 A and 1200 V) was chosen as diodes ($D_{rec1} - D_{rec4}$, D_{aux1} and D_{aux2}) by using 2 of RHRP30120 diode connected in series to support the secondary reverse voltage in practice. For the design of the auxiliary capacitor (C_{aux}) to achieve the ZCS condition, it can consider in the resetting time mode as shown in the Figure 4(b). In this interval, the ZCS condition can be achieved for MOSFETs (S_2 and S_3) if the stored energy in C_{aux} is greater than the stored energy in L_{lk} of the high frequency transformer. The condition of ZCS can be given by (6).

$$\frac{1}{2} C_{aux} V_{c,aux}^2 \geq \frac{1}{2} \frac{L_{lk}}{n^2} I_o^2 \quad (6)$$

In the retting time mode, the auxiliary capacitor voltage ($V_{c,aux}$) equals to the $V_{dc,bus}$. Therefore, the value of the auxiliary capacitor (C_{aux}) can be calculated by (7).

$$C_{aux} \geq L_{lk} \left(\frac{I_o}{V_o n}\right)^2 = 48.7\ nF \quad (7)$$

According to (7), the value of the auxiliary capacitor (C_{aux}) should be larger than 48.7 nF. Thus, the value of 2 μF was chosen to guarantee the ZCS condition.

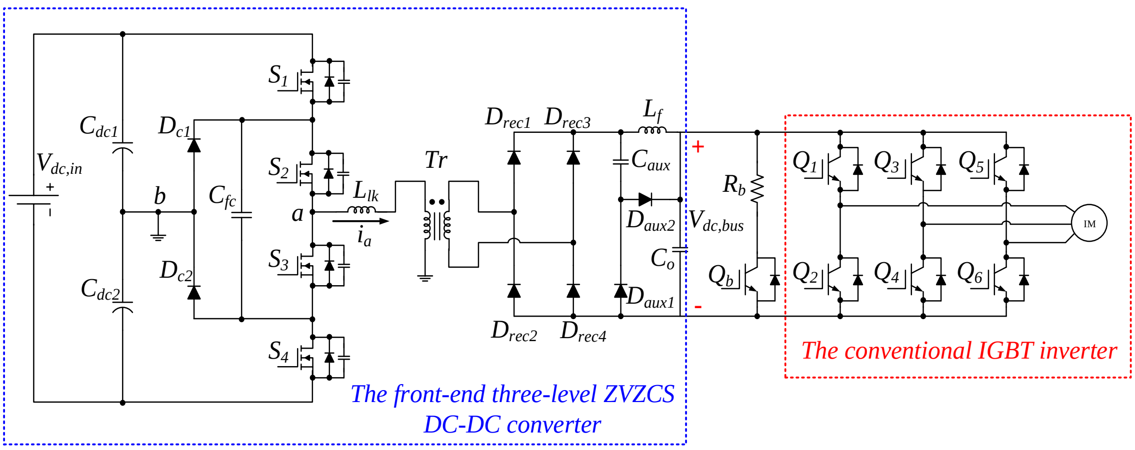

Figure 2. The power conversion circuit in this research

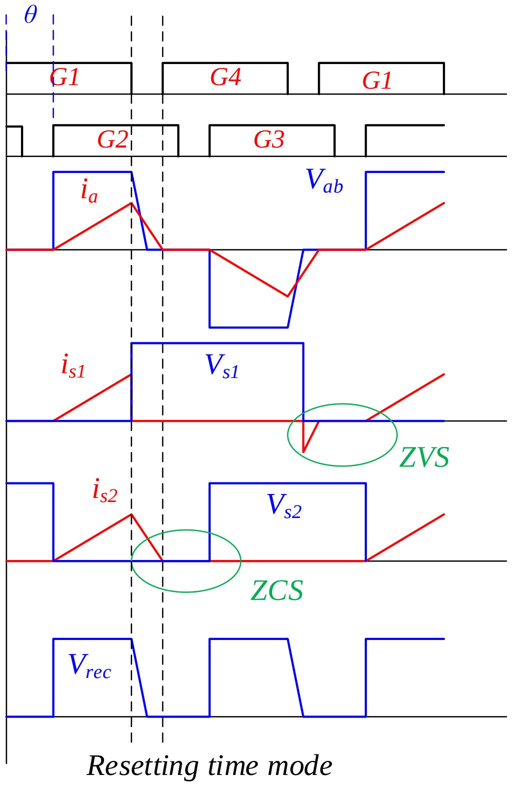

Figure 3. Some waveforms of the front-end converter

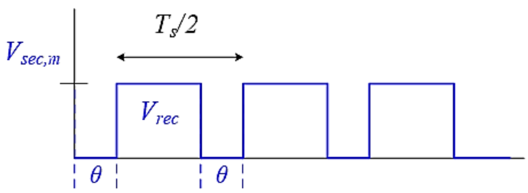

(a)

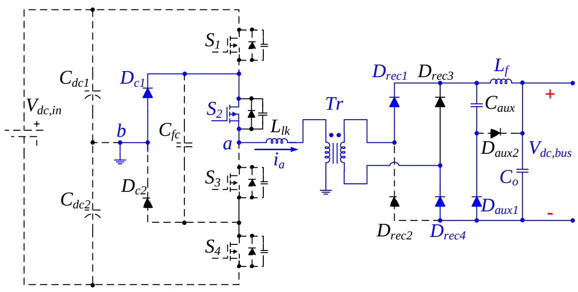

(b)

Figure 4. The analysis of resetting time mode (a) ideal rectified voltage waveform and (b) the retting time mode

2.4. The IoT system in this research

According to Figure 5, the IoT system for the paddle wheel machine consists of main parts as follows: i) Inverter connection port is used to send important signals for operating the VFD inverter to control the frequency and speed of the paddle wheel machine; ii) LCD panel is used for monitoring all data in this research; iii) Keypad is installed for getting the command from the farmer in the manual mode; and iv) Remote communication port is used for communicating via the mobile system of the farmer. In this research, Raspberry Pi 4 Model B is selected to be the processor unit for controlling the hardware unit. Figure 6 reveals the Node-RED software which is developed for controlling the IoT VFD inverter by using the Python V.3 language to send the command to hardware in the IoT system. All measured data such as the operation mode, on-off time, and the speed of the paddle wheel machine are collected in the MySQL and influx database. In addition, the Node-RED software is used for developing the communication part for the farmer via the web application which can be illustrated in Figure 7.

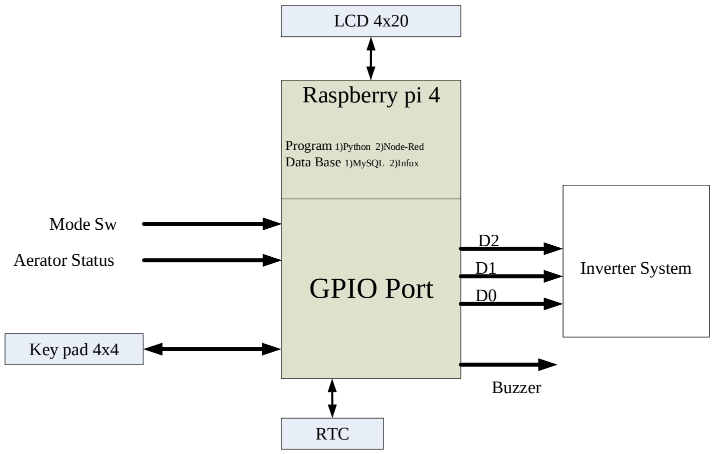

Figure 5. IoT system in this research

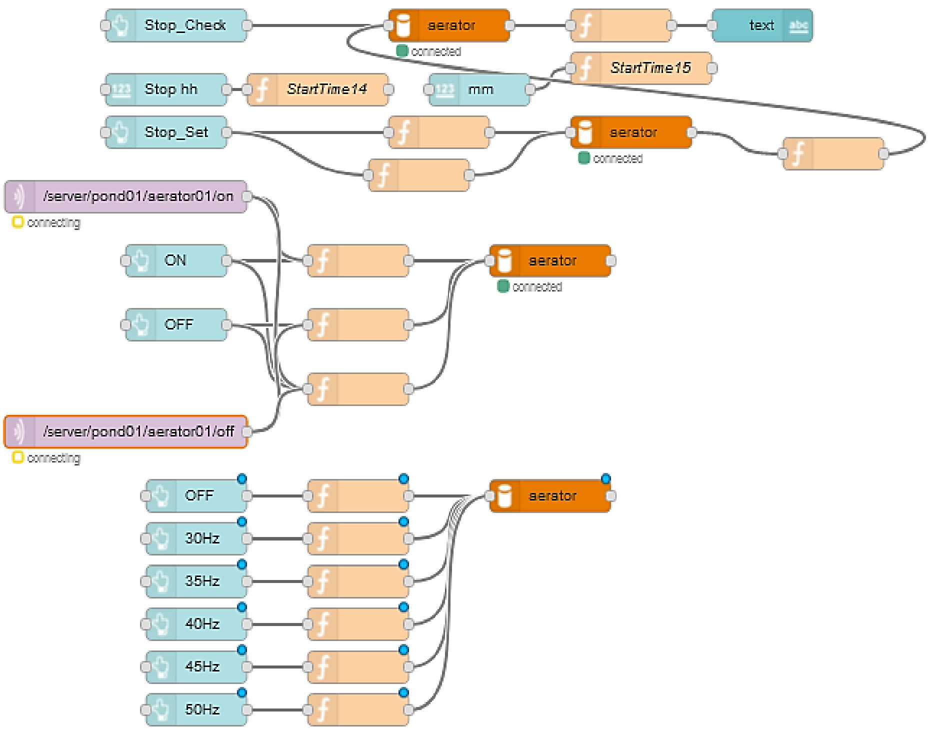

Figure 6. The development of the Node-RED software

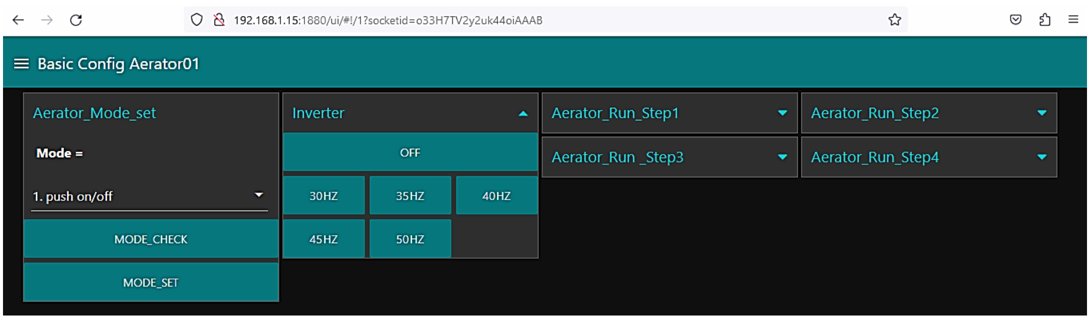

Figure 7. User interface developed by the Node-RED software

There are 3 output bits from the IoT system which connected with the inverter for adjusting the frequency of the induction motor as illustrated in Table 1. From Figure 7, there are 2 modes for controlling the paddle wheel machine which can be chosen by a Mode SW button. The first mode is the normal mode for operating and adjusting the speed of the motor by using the inverter at the fieldwork or via the smartphone.

Table 1. The output bits from the IoT system for commanding the VFD inverter

Case	Frequency (Hz)	D2	D1	D0
1	0	0	0	0
2	30	0	0	1
3	35	0	1	0
4	40	0	1	1
5	45	1	0	0
6	50	1	0	1

3. RESULTS AND DISCUSSION

In order to confirm the effectiveness of the front-end three-level ZVZCS DC-DC converter while operating with the VFD inverter for the paddle wheel machine in the shrimp pond. The prototype of the front-end converter was built and tested in the laboratory and the fieldwork. Some experimental results of the proposed circuit can be illustrated by using the parameters in Table 2. Figures 8-11 illustrate the voltage and the current waveforms of all switches (S_1; S_2; S_3; and S_4, respectively) in the front-end ZVZCS DC-DC converter. It was found that, switches S_1 and S_4 can meet the ZVS condition at turning on time of while the ZCS condition occurs at turning off time of switches S_2 and S_3. Thus, the switching loss can be eliminated significantly.

Table 2. Parameters of the front-end converter

Parameters	Value
Rated power	3 kW
Rated DC input voltage ($V_{dc,in}$)	540 V
Rated DC bus voltage ($V_{dc,bus}$)	700 V
Switching frequency (f_{sw})	65 kHz
Turn ratio of transformer, T_r (n)	5:38
Leakage inductor (L_{lk})	22 μH
Auxiliary capacitor (C_{aux})	2 μF

Furthermore, the voltage stress on switches equals to $V_{dc,in}/2$ because of the use of three-level topology as an inverter part of the front-end converter. Figure 12 shows the voltage and the current waveforms at the primary side of the high frequency transformer (T_r) at 60 degree of phase-shifted angle and 100% of the output load. Figures 13 and 14 indicate the DC voltage and the DC current waveforms at the input and output sides of the front-end converter at rated voltage and rated power. Figure 15 shows the graph of the relationship between the total efficiency of the front-end converter and the percentage of the output load at 2 μF of the auxiliary capacitor (C_{aux}). It can be observed that, the maximum efficiency of the front-end converter is 94.9% at 75% of a full load. In addition, Figures 16 and 17 show the measured output waveforms of the VFD inverter by receiving the DC bus voltage from the front-end converter at 700 V. Finally, the power conversion circuit was installed at the fieldwork as shown in Figure 18 to confirm the possibility and the effectiveness the system.

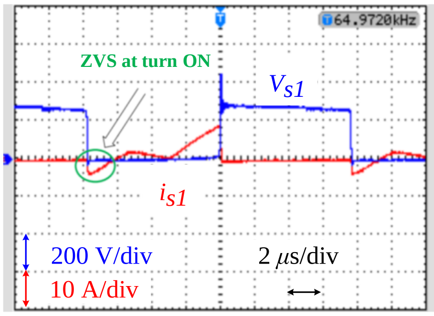

Figure 8. Voltage and current waveforms of S_1

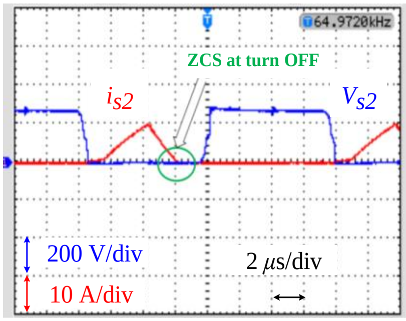

Figure 9. Voltage and current waveforms of S_2

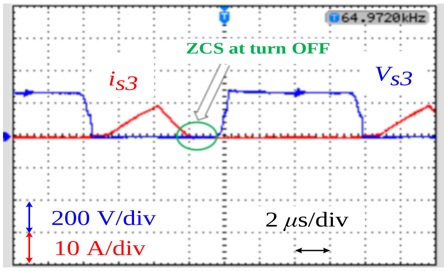

Figure 10. Voltage and current waveforms of S_3

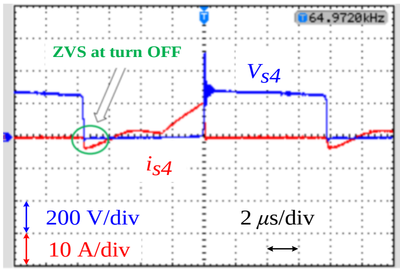

Figure 11. Voltage and current waveforms of S_4

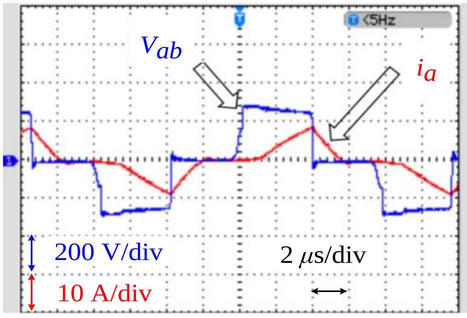

Figure 12. Primary voltage and current waveforms at 60 degree of phase-shifted angle (θ)

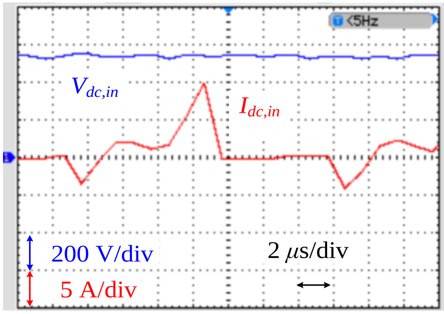

Figure 13. Input voltage and current waveforms

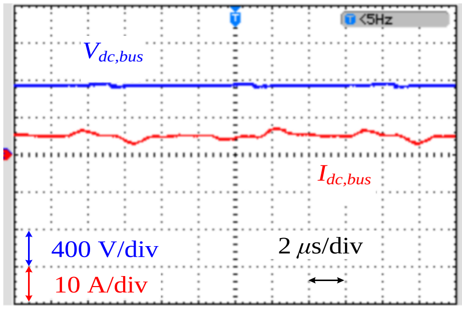

Figure 14. Output voltage and current waveforms

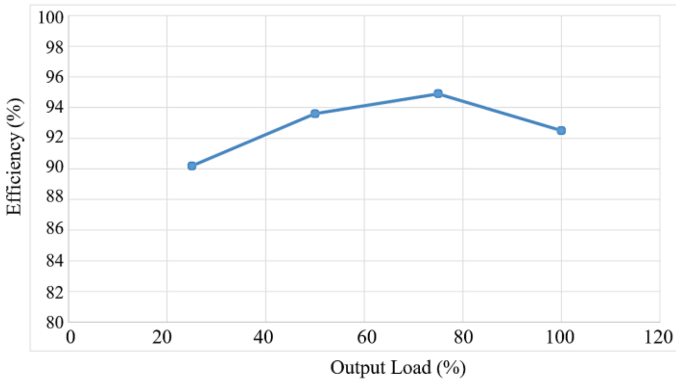

Figure 15. The relationship graph between the total efficiency and the percentage of the output load

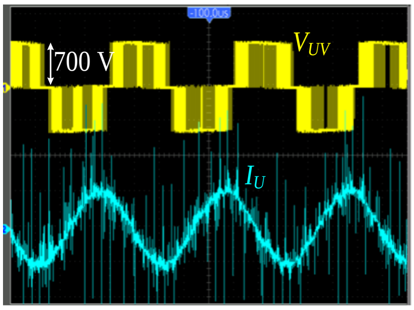

Figure 16. Output voltage (V_{uv}, 500 V/div) and current of the VFD inverter (I_u, 5A/div)

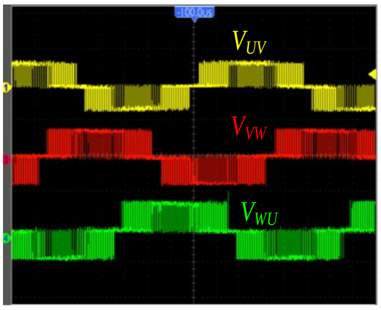

Figure 17. Line to line voltage of the VFD inverter (V_{uv}, V_{vw} and V_{wu}; 1000 V/div)

Figure 18. The research fieldwork (shrimp farm)

4. CONCLUSION

This research paper has presented the integration of power electronics together with IoT technologies for applying in shrimp farming. This paper focuses on the design of the proposed front-end 3L ZVZCS DC-DC converter to supply the DC bus voltage to the VFD inverter for the induction motor of the paddle wheel machine in the shrimp pond. The proposed circuit was installed and tested as illustrated in the experimental results with around 70 days of the runtime. It can be observed that, the front-end converter can step up the DC bus voltage to 700 V which is enough for operating the VFD inverter. All switches in the circuit can completely achieve the ZVZCS condition resulting in decreasing switching losses and increasing the reliability of the circuit. The proposed front-end converter can provide 94.9% of the maximum experimental efficiency at 75% of a full load and the cost effectiveness of the front-end converter is about 8,000 THB per inverter set.

ACKNOWLEDGEMENTS

Authors would like to thank Thailand Science Research and Innovation (TSRI) for the support of the research funding of this research through Nakhon Pathom Rajabhat University.

REFERENCES

[1] M. Ćalasan, M. Alqarni, M. Rosić, N. Koljčević, B. Alamri, and S. H. E. A. Aleem, "A Novel Exact Analytical Solution Based on Kloss Equation towards Accurate Speed-Time Characteristics Modeling of Induction Machines during No-Load Direct Startups," *Appl. Sci.*, vol. 11, no. 11, p. 5102, May 2021, doi: 10.3390/app11115102.

[2] M. S. Shaikh, S. Raj, R. Babu, S. Kumar, and K. Sagrolikar, "A hybrid moth–flame algorithm with particle swarm optimization with application in power transmission and distribution," *Decis. Anal. J.*, vol. 6, no. 4, p. 100182, Mar. 2023, doi: 10.1016/j.dajour.2023.100182.

[3] M. S. Shaikh, S. Raj, M. Ikram, and W. Khan, "Parameters estimation of AC transmission line by an improved moth flame optimization method," *J. Electr. Syst. Inf. Technol.*, vol. 9, no. 1, p. 25, Dec. 2022, doi: 10.1186/s43067-022-00066-x.

[4] M. S. Shaikh, C. Hua, M. A. Jatoi, M. M. Ansari, and A. A. Qader, “Application of grey wolf optimisation algorithm in parameter calculation of overhead transmission line system,” *IET Sci. Meas. Technol.*, vol. 15, no. 2, pp. 218–231, Mar. 2021, doi: 10.1049/smt2.12023.

[5] M. Suhail Shaikh *et al.*, “Optimal parameter estimation of 1-phase and 3-phase transmission line for various bundle conductor’s using modified whale optimization algorithm,” *Int. J. Electr. Power Energy Syst.*, vol. 138, p. 107893, Jun. 2022, doi: 10.1016/j.ijepes.2021.107893.

[6] M. S. Shaikh, C. Hua, M. Hassan, S. Raj, M. A. Jatoi, and M. M. Ansari, “Optimal parameter estimation of overhead transmission line considering different bundle conductors with the uncertainty of load modeling,” *Optim. Control Appl. Methods*, vol. 43, no. 3, pp. 652–666, May 2021, doi: 10.1002/oca.2772.

[7] M. Karami, T. Li, R. Tallam, and R. Cuzner, “Thermal Characterization of SiC Modules for Variable Frequency Drives,” *IEEE Open J. Power Electron.*, vol. 2, pp. 336–345, 2021, doi: 10.1109/OJPEL.2021.3075441.

[8] M. Van Chung, D. T. Anh, and P. Vu, “A finite set-model predictive control based on FPGA flatform for eleven-level cascaded H-Bridge inverter fed induction motor drive,” *Int. J. Power Electron. Drive Syst.*, vol. 12, no. 2, pp. 845–857, Jun. 2021, doi: 10.11591/ijpeds.v12.i2.pp845-857.

[9] V. T. Ha and P. T. Giang, “Control for induction motor drives using predictive model stator currents and speeds control,” *Int. J. Power Electron. Drive Syst.*, vol. 13, no. 4, pp. 2005–2013, Dec. 2022, doi: 10.11591/ijpeds.v13.i4.pp2005-2013.

[10] M. S. Shaikh, C. Hua, M. A. Jatoi, M. M. Ansari, and A. A. Qader, “Parameter Estimation of AC Transmission Line Considering Different Bundle Conductors Using Flux Linkage Technique,” *IEEE Can. J. Electr. Comput. Eng.*, vol. 44, no. 3, pp. 313–320, 2021, doi: 10.1109/ICJECE.2021.3069143.

[11] Y. Liu and F. Z. Peng, “Fast control of PWAM boost-converter-inverter system for HEV/EV motor drives,” in *2014 IEEE Applied Power Electronics Conference and Exposition - APEC 2014*, IEEE, Mar. 2014, pp. 2446–2452. doi: 10.1109/APEC.2014.6803646.

[12] A. Janabi and B. Wang, “Switched-Capacitor Voltage Boost Converter for Electric and Hybrid Electric Vehicle Drives,” *IEEE Trans. Power Electron.*, vol. 35, no. 6, pp. 5615–5624, Jun. 2020, doi: 10.1109/TPEL.2019.2949574.

[13] J. R. Garcia-Sánchez *et al.*, “A Robust Differential Flatness-Based Tracking Control for the ‘MIMO DC/DC Boost Converter–Inverter–DC Motor’ System: Experimental Results,” *IEEE Access*, vol. 7, pp. 84497–84505, 2019, doi: 10.1109/ACCESS.2019.2923701.

[14] M. A. N. Amran, A. A. Bakar, M. H. A. Jalil, A. F. H. A. Gani, and E. Pathan, “Optimal tuning of PI controller using system identification for two-phase boost converter for low-voltage applications,” *Int. J. Power Electron. Drive Syst.*, vol. 12, no. 4, pp. 2393–2402, Dec. 2021, doi: 10.11591/ijpeds.v12.i4.pp2393-2402.

[15] H. Jedi and G. A. Hussain, “A 1 MHz soft-switching boost DC-DC converter with matching network,” *Int. J. Power Electron. Drive Syst.*, vol. 13, no. 4, pp. 2226–2234, Dec. 2022, doi: 10.11591/ijpeds.v13.i4.pp2226-2234.

[16] H. Wu, T. Mu, H. Ge, and Y. Xing, “Full-Range Soft-Switching-Isolated Buck-Boost Converters With Integrated Interleaved Boost Converter and Phase-Shifted Control,” *IEEE Trans. Power Electron.*, vol. 31, no. 2, pp. 987–999, Feb. 2016, doi: 10.1109/TPEL.2015.2425956.

[17] M. M. Ansari, C. Guo, M. S. Shaikh, N. Chopra, I. Haq, and L. Shen, “Planning for Distribution System with Grey Wolf Optimization Method,” *J. Electr. Eng. Technol.*, vol. 15, pp. 1485–1499, Jul. 2020, doi: 10.1007/s42835-020-00419-4.

[18] Z. Zhou, H. Li, and X. Wu, “A Constant Frequency ZVS Control System for the Four-Switch Buck–Boost DC–DC Converter With Reduced Inductor Current,” *IEEE Trans. Power Electron.*, vol. 34, no. 7, pp. 5996–6003, Jul. 2019, doi: 10.1109/TPEL.2018.2884950.

[19] Y. Yan, H. Gui, and H. Bai, “Complete ZVS Analysis in Dual Active Bridge,” *IEEE Trans. Power Electron.*, vol. 36, no. 2, pp. 1247–1252, Feb. 2021, doi: 10.1109/TPEL.2020.3011470.

[20] Q. Huang and A. Q. Huang, “Variable Frequency Average Current Mode Control for ZVS Symmetrical Dual-Buck H-Bridge All-GaN Inverter,” *IEEE J. Emerg. Sel. Top. Power Electron.*, vol. 8, no. 4, pp. 4416–4427, Dec. 2020, doi: 10.1109/JESTPE.2019.2940270.

[21] D. Liu, Y. Wang, Q. Zhang, and Z. Chen, “ZVZCS Full-Bridge Three-Level DC/DC Converter With Reduced Device Count,” *IEEE Trans. Power Electron.*, vol. 35, no. 10, pp. 9965–9970, Oct. 2020, doi: 10.1109/TPEL.2020.2977227.

[22] R. H. Ashique and Z. Salam, “A Family of True Zero Voltage Zero Current Switching (ZVZCS) Nonisolated Bidirectional DC–DC Converter With Wide Soft Switching Range,” *IEEE Trans. Ind. Electron.*, vol. 64, no. 7, pp. 5416–5427, Jul. 2017, doi: 10.1109/TIE.2017.2669884.

[23] T. Song, N. Huang, and A. Ioinovici, “A family of zero-voltage and zero-current-switching (ZVZCS) three-level DC-DC converters with secondary-assisted regenerative passive snubber,” *IEEE Trans. Circuits Syst. I Regul. Pap.*, vol. 52, no. 11, pp. 2473–2481, Nov. 2005, doi: 10.1109/TCSI.2005.853911.

[24] H. T. Thong, N. H. Linh, H. Van Canh, P. V. Phuong, and N. K. Trung, “Unbalanced three-phase interleaved LLC resonant converter: current phase angle balancing technique,” *Int. J. Power Electron. Drive Syst.*, vol. 13, no. 2, pp. 1056–1067, Jun. 2022, doi: 10.11591/ijpeds.v13.i2.pp1056-1067.

[25] H. Li, L. Zhao, C. Xu, and X. Zheng, “A Dual Half-Bridge Phase-Shifted Converter With Wide ZVZCS Switching Range,” *IEEE Trans. Power Electron.*, vol. 33, no. 4, pp. 2976–2985, Apr. 2018, doi: 10.1109/TPEL.2017.2711618.

[26] J. G. Cho, J. W. Baek, C. Y. Jeong, D. W. Yoo, H. S. Lee, and G. H. Rim, “Novel zero-voltage and zero-current-switching (ZVZCS) full bridge PWM converter using a simple auxiliary circuit,” in *APEC ’98 Thirteenth Annual Applied Power Electronics Conference and Exposition*, IEEE, 1998, pp. 834–839. doi: 10.1109/APEC.1998.653995.

[27] A. Mousavi and G. Moschopoulos, “A New ZCS-PWM Full-Bridge DC–DC Converter With Simple Auxiliary Circuits,” *IEEE Trans. Power Electron.*, vol. 29, no. 3, pp. 1321–1330, Mar. 2014, doi: 10.1109/TPEL.2013.2259847.

[28] F. Liu, J. Yan, and X. Ruan, “Zero-Voltage and Zero-Current-Switching PWM Combined Three-Level DC/DC Converter,” *IEEE Trans. Ind. Electron.*, vol. 57, no. 5, pp. 1644–1654, May 2010, doi: 10.1109/TIE.2009.2031950.

[29] T. T. Song, N. Huang, and A. Ioinovici, “A Zero-Voltage and Zero-Current Switching Three-Level DC–DC Converter With Reduced Rectifier Voltage Stress and Soft-Switching-Oriented Optimized Design,” *IEEE Trans. Power Electron.*, vol. 21, no. 5, pp. 1204–1212, Sep. 2006, doi: 10.1109/TPEL.2006.880351.

[30] S. K. Yadav, N. Mishra, B. Singh, S. Padmanaban, and F. Blaabjerg, “Scott-Tied Magnetically Linked Solar Multilevel Converter in Varying Environmental Conditions,” *IEEE J. Emerg. Sel. Top. Ind. Electron.*, vol. 3, no. 3, pp. 559–571, Jul. 2022, doi: 10.1109/JESTIE.2022.3154714.

[31] T. A. Hussein, “Multilevel level single phase inverter implementation for reduced harmonic contents,” *Int. J. Power Electron. Drive Syst.*, vol. 12, no. 1, p. 314-324, Mar. 2021, doi: 10.11591/ijpeds.v12.i1.pp314-324.

[32] K. Himour and K. Iffouzar, "A random PWM control strategy for a three level inverter used in a grid connected photovoltaic system," *Int. J. Power Electron. Drive Syst.*, vol. 11, no. 3, pp. 1547–1556, Sep. 2020, doi: 10.11591/ijpeds.v11.i3.pp1547-1556.

[33] P. Mayer, M. Magno, and L. Benini, "Smart Power Unit—mW-to-nW Power Management and Control for Self-Sustainable IoT Devices," *IEEE Trans. Power Electron.*, vol. 36, no. 5, pp. 5700–5710, May 2021, doi: 10.1109/TPEL.2020.3031697.

[34] S. Carreon-Bautista, L. Huang, and E. Sanchez-Sinencio, "An Autonomous Energy Harvesting Power Management Unit With Digital Regulation for IoT Applications," *IEEE J. Solid-State Circuits*, vol. 51, no. 6, pp. 1457–1474, Jun. 2016, doi: 10.1109/JSSC.2016.2545709.

[35] S. Mondal and R. Paily, "On-Chip Photovoltaic Power Harvesting System With Low-Overhead Adaptive MPPT for IoT Nodes," *IEEE Internet Things J.*, vol. 4, no. 5, pp. 1624–1633, Oct. 2017, doi: 10.1109/JIOT.2017.2692383.

[36] M. N. Kamarudin, S. M. Rozali, and M. S. Jamri, "Active cooling photovoltaic with IoT facility," *Int. J. Power Electron. Drive Syst.*, vol. 12, no. 3, pp. 1494–1504, Sep. 2021, doi: 10.11591/ijpeds.v12.i3.pp1494-1504.

[37] E. Muchtar, E. Sanjaya, and F. I. Hariadi, "Human machine interface on e-Shrimp as smart control system for whiteleg shrimp pond," in *2017 International Symposium on Electronics and Smart Devices (ISESD)*, IEEE, Oct. 2017, pp. 24–29. doi: 10.1109/ISESD.2017.8253299.

[38] W. Cheunta, N. Chirdchoo, and K. Saelim, "Efficiency improvement of an integrated giant freshwater-white prawn farming in Thailand using a Wireless Sensor Network," in *Signal and Information Processing Association Annual Summit and Conference (APSIPA), 2014 Asia-Pacific*, IEEE, Dec. 2014, pp. 1–5. doi: 10.1109/APSIPA.2014.7041774.

[39] C. Zhang, Z. Gao, T. Chen, and J. Yang, "Isolated DC/DC converter with three-level high-frequency link and bidirectional power flow ability for electric vehicles," *IET Power Electron.*, vol. 12, no. 7, pp. 1742–1751, June. 2019, doi: 10.1049/iet-pel.2018.6268.

BIOGRAPHIES OF AUTHORS

Nitthita Chirdchoo received her B.Eng. (Hons.) degree in telecommunication engineering from the Suranaree University of Technology, Thailand, in 1999. In 2000, she was awarded the scholarship by the Royal Thai Government to study at the University of Pittsburgh, USA, where she obtained her M.Sc. degree in Telecommunication in 2002. After obtaining her M.Sc. degree, she started her academic career as a lecturer in Telecommunication Engineering at Nakhon Pathom Rajabhat University, Thailand. In 2005, she was granted a Research Scholarship from the National University of Singapore, where she received the Ph.D. degree in Electrical & Computer Engineering in 2010. Since 2010, she has continued her career with the Department of Electrical Engineering, Faculty of Science and Technology, Nakhon Pathom Rajabhat University, Thailand. Her research interests are in underwater acoustic networks, wireless sensor networks, deep learning and computer vision, smart farming, and UWB precise indoor localization and applications. She can be contacted at email: nitthita@webmail.npru.ac.th.

Watanyu Meesrisuk received his B.Eng., M.Eng., and D.Eng. in electrical engineering from King Mongkut's Institute of Technology Ladkrabang, Bangkok, Thailand, in 2013, 2014, and 2017, respectively. He is an assistant professor at Department of Electrical Engineering, Nakhon Pathom Rajabhat University, Thailand. His current research interests include DC-DC Converters, switching power supply and applications of power electronics. He can be contacted at email: watanyu@webmail.npru.ac.th.

Weerasak Chuenta received his B.S. in Industrial Computer (Industrial Electronics Technology) from Ubon Ratchathani Rajabhat University, Ubon Ratchathani, Thailand in 1995. He earned an M.S. in Technical Education from King Mongkut's University of Technology Thonburi, Bangkok, Thailand, in 1995. His research areas of interest lie in indoor localization and tracking, computer vision and image processing, IoT applications, precision farming, and smart farming systems. He can be contacted at email: weerasak@webmail.npru.ac.th.